White organic light-emitting devices based on phosphor-sensitized fluorescence*

ZOU Wenjing[1], ZHAO Yukang[1], WU Youzhi[1,*], ZHANG Cairong[2]

1. School of Materials Science & Engineering, Lanzhou University of Technology, Lanzhou 730050, China
2. School of Science, Lanzhou University of Technology, Lanzhou 730050, China

Abstract

Although phosphorescent organic light-emitting devices (OLEDs) can have an internal quantum efficiency (IQE) of 100%, the IQE usually decays at high current densities due to triplet-triplet annihilation. Phosphor-sensitized fluorescence can realize the energy transfer between phosphorescent emitter and fluorescent emitter, and can be used to suppress the efficiency fluctuations and adjust the color of the device. With this in mind, white light emission including different colors of phosphorescent emitter and fluorescent emitter can be expected. Herein, phosphor-sensitized fluorescent white OLEDs are fabricated by combining ultra-thin layer insertion and doping, in which laser dyes DCM (4-(Dicyanomethylene)-2-methyl-6-(4-dimethyl-aminostyryl)-4H-pyran), iridium complexes $Ir(ppy)_3$ (tris(2-phenylpyridine)iridium), and biphenyl ethylene derivatives BCzVB (1,4-bis[2- (3-N-ethylcarbazoryl)vinyl]benzene) are used as red, green and blue emitters, respectively. By adjusting the doping concentration of $Ir(ppy)_3$ phosphorescent green emitter in CBP (4,4'-N,N'-dicarbazole-biphyenyl) host, with ultra-thin layers of BCzVB fluorescent blue emitter on both sides of CBP:$Ir(ppy)_3$ doping system and with ultra-thin layer of DCM fluorescent red emitter inserting in CBP:$Ir(ppy)_3$ layer, the three colors can be balanced. White emissions are obtained in the device, the highest external quantum efficiency is 2.5% (current efficiency of 5.1 cd/A), the maximum brightness is 12400 cd/m^2, and Commission Internationale de l'Eclairage (CIE) co-ordinates can reach the ideal white light equilibrium point (0.33, 0.33) at a current density of 1 mA/cm^2. The acquisition of white light is attributed to the appropriate doping ratio of $Ir(ppy)_3$ and the position of DCM, which effectively balances the emission ratio of three primary colors: red, green, and blue. The results indicate that the partially energy transfer of triplet excitons to singlet excitons by phosphor-sensitized fluorescence scheme can be used to realize high-efficiency white organic electroluminescent devices, thereby reducing energy consumption and providing more room for promoting OLED applications.

* The paper is an English translated version of the original Chinese paper published in *Acta Physica Sinica*. Please cite the paper as: ZOU Wenjing, ZHAO Yukang, WU Youzhi, ZHANG Cairong, White organic light-emitting devices based on phosphor-sensitized fluorescence. *Acta Phys. Sin.*, 2025, 74(2): 028101. doi: 10.7498/aps.74.20241294

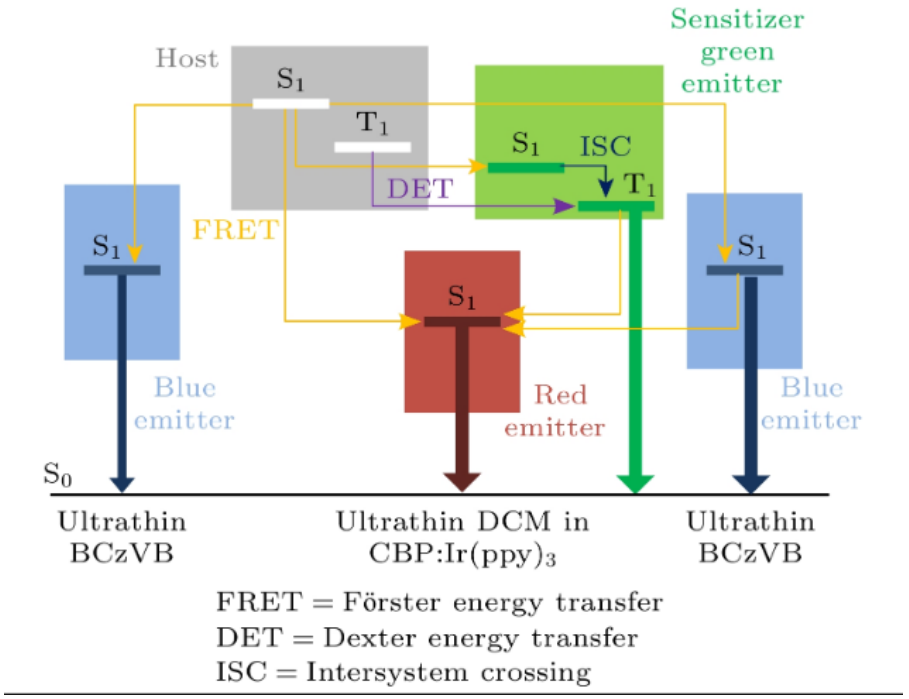

Keywords: organic light-emitting devices; phosphor-sensitized fluorescence; ultrathin layer; laser dyes

PACS:

81.05.Fb (Organic semiconductors)

78.47.da (Excited states)

34.50.Ez (Rotational and vibrational energy transfer)

doi: 10.7498/aps.74.20241294
cstr: 32037.14.aps.74.20241294

1. Introduction

(Organic light-emitting devices, OLEDs) have become a hot[1–4] for next-generation full-color displays and solid-state lighting due to their high brightness, high contrast, wide viewing angle, and excellent color tunability. In the early days, OLED were often prepared with fluorescent materials. Because fluorescent materials can only harvest singlet excitons, the theoretical maximum internal quantum efficiency of all-fluorescent OLED is only 25%, corresponding to an external quantum efficiency of about 5%[5,6], which seriously restricts the improvement of OLED efficiency. Later, phosphorescent OLED were noticed, because phosphorescent materials can use both singlet excitons and triplet excitons to emit light, thus theoretically achieving 100% internal quantum efficiency[7,8]. However, triplet excitons have a long lifetime, and the accumulation of triplet excitons in phosphorescent devices at high current density causes triplet-triplet annihilation TTA[9,10], resulting in a rapid decline in device efficiency[11,12]. If a fast and effective

energy transfer channel can be established between phosphorescent and fluorescent materials to transfer the accumulated triplet exciton energy to the fluorescent material, taking advantage of the short lifetime and fast energy release rate of singlet excitons in fluorescent materials, this can significantly reduce triplet exciton accumulation, suppress TTA, improve triplet exciton utilization, and ultimately enhance device luminescence performance. Based on this consideration, researchers have studied phosphorescence-sensitized fluorescence[13,14], which can realize the energy transfer between phosphorescence and fluorescent materials, and realize the energy transfer from triplet excitons in phosphorescent materials to singlet excitons in fluorescent materials, thus greatly improving the luminous efficiency of devices.

Baldo et al.[13] realized phosphorescence-sensitized fluorescence by alternately doping a phosphorescence-sensitizer $Ir(ppy)_3$ (Tris (2-phenylpyridine) iridium) and a fluorescent material DCM2 on a thin layer of a host material CBP (4,4′-N,N′-dicarbazole-biphyenyl), and the external quantum efficiency of the device was increased from 0.9% to 3.7%. D 'Andrade et al.[15] realized phosphorescence-sensitized fluorescence by uniformly co-doping two luminescent materials into the host material, improved and simplified the process of Baldo et al.[13], and proved that the Förster energy transfer between $Ir(ppy)_3$ and DCM2 could be up to 100%, and the external quantum efficiency was increased to 9%. This shows that phosphorescence sensitized fluorescence is feasible. Heimel et al.[14] prepared an efficient and stable sky-blue monochromatic light-emitting device based on phosphorescence-sensitized fluorescence, which not only reduced the radiation decay time of the phosphorescent material, but also retained the light-emitting color of the phosphorescent material, and its operating lifetime (80% of the initial brightness of 1000 cd/m^2) reached 320 hrs., opening up a new idea for the research of efficient and stable blue light-emitting devices. In recent years, references [16-18] have reported that phosphorescence-sensitized fluorescence is also used in thermally activated delayed fluorescence (TADF) devices to improve the device performance, and the efficiency and color purity are further improved, but the inherent slow response and stability problems of TADF devices have not been greatly changed. In addition, phosphorescent sensitizer and TADF emitter are doped into a host material at the same time, which increases the cost of device preparation. Because it is difficult to accurately control the evaporation rate of the host and guest materials in the actual operation of the doping process, thus affecting the doping ratio of the film, especially when two guest materials are doped in the host material at the same time, the control is more difficult. If one of the guest materials is inserted into a host material and the other guest doped layer by means of an ultra-thin layer[19,20], the device preparation process can be simplified and the doping effect can also be achieved.

In this paper, the high efficiency of phosphorescent materials is used to make full use of singlet and triplet exciton energy, and the red, green and blue components are expected to appear simultaneously in the device to obtain white light. Based on this, CBP was used as the host material, and the green phosphorescent material $Ir(ppy)_3$ was doped into CBP by the conventional method, which was used as the green component of white light devices; A red fluorescent material

DCM (4-(Dicyanomethylene)-2-methyl-6-(4-dimethyl- aminostyryl)-4H-pyran), which is similar to DCM2 in structure and performance, is inserted into the CBP:Ir(ppy)$_3$ layer in an ultra-thin layer mode to be used as a red light component; The blue fluorescent material BCzVB (1,4-bis[2-(3-N-ethylcarbazoryl)vinyl]benzene) was also placed on both sides of the CBP:Ir(ppy)$_3$ layer in an ultrathin-layer form, i.e., at the TAPC (1,1-bis((di-4-tolylamino)phenyl)cyclohexane)/ CBP:Ir(ppy)$_3$ and the CBP:Ir(ppy)$_3$/TPBi(1,3,5-tris(1-phenyl-1H-benzimidazol-2-yl)benzene interfaces. The highest external quantum efficiency is 2.5% (current efficiency is 5.1 cd/A), and the device with the DCM ultrathin layer located at 12 nm from the TAPC/CBP:Ir(ppy)$_3$ interface has a Commission Internationale de l'Eclairage (Commission Internationale de L 'Eclairage, CIE) coordinate of (0.33, 0.33) at a current density of 1 mA/cm^2, reaching the ideal white light equilibrium point.

2. Experiment

Vacuum thermal evaporation process is used for device fabrication. The surface of (indium tin oxide, ITO) conductive glass with a sheet resistance of 50 Ω/square was treated to a hydrophilic state by cleaning agent, and then the glass substrate was immersed in acetone, ethanol and deionized water for ultrasonic cleaning for 15 min, respectively. Finally, the substrate was dried by an infrared dryer and placed in a vacuum chamber. The mechanical pump and the molecular pump are used together to make the vacuum chamber reach a high vacuum state, about 6×10^{-4} Pa. According to the device structure fabrication requirements, selective thermal evaporation of MoO_3, TAPC, BCzVB, CBP:Ir(ppy)$_3$, DCM, TPBi, LiF and Al are respectively used as a hole injection layer, a hole transport layer, a blue fluorescent light emitting layer, a green phosphorescent material doped light emitting layer and a red fluorescent light emitting layer, an electron transport and hole blocking layer, an electron injection layer and a cathode. Fig. 1 is the chemical structure of the above organic materials, Fig. 2 is the device structure and energy level diagram, and the energy level data are taken from the literatures [21–26]. First, the fabricated device structure is: ITO/MoO_3 (0.05 nm)/TAPC (50 nm)/BCzVB (0.3 nm)/CBP: Ir(ppy)$_3$ (x%, 20 nm)/TPBi (20 nm)/LiF (1.5 nm)/Al, x = 6, 3, 1, 0.7, 0.4, and the corresponding devices are marked as A1, A2, A3, A4 and A5, respectively. Unless otherwise specified, the doping concentrations mentioned in the following text are all mass fractions. The suitable doping concentration of Ir(ppy)$_3$ is 0.7%. Secondly, the insertion position of DCM was optimized, and the fabricated device structure was: ITO/MoO_3 (0.05 nm)/TAPC (50 nm)/BCzVB (0.3 nm)/CBP:Ir(ppy)$_3$ (0.7%, y nm)/DCM (0.3 nm)/CBP:Ir(ppy)$_3$ (0.7%, 20 – y nm)/BCzVB (0.3 nm)/TPBi (20 nm)/LiF (1.5 nm)/Al, y = 10, 12, 14, 16. The distance of DCM from the BCzVB/CBP:Ir(ppy)$_3$ interface at the anode side is denoted as B1, B2, B3, and B4 for the corresponding devices. The insertion position of DCM is determined to be y = 12 nm. Note that the thicknesses of MoO_3 (0.05 nm) and BCzVB (0.3 nm) in the devices were optimized and determined, as detailed in Ref. [27]. Additionally, the thickness of DCM was also optimized and found to be similar to the optimal BCzVB thickness, remaining at 0.3 nm.

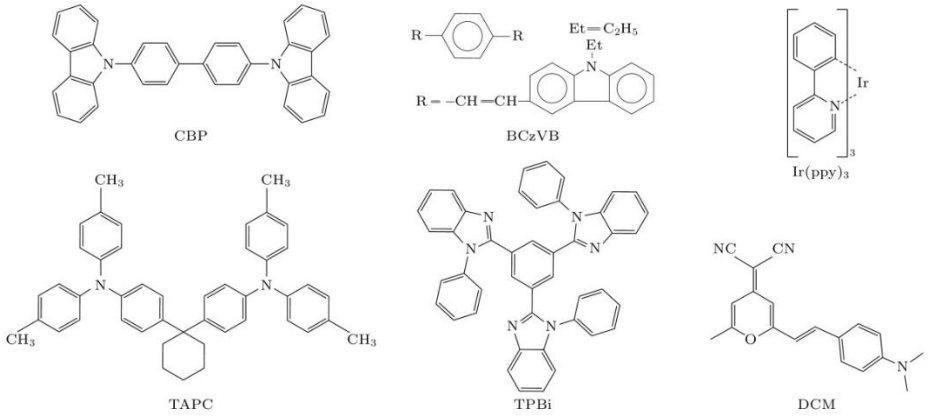

Figure 1. The chemical structure of organic materials

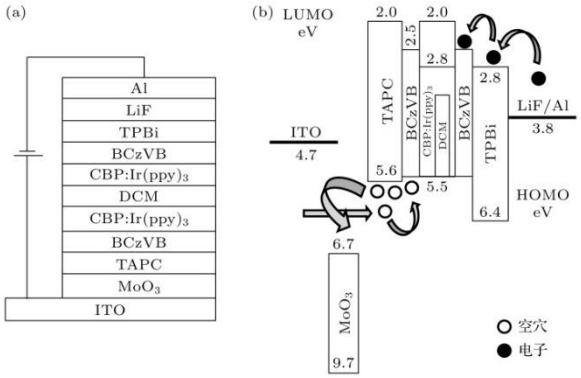

Figure 2. Schematic diagram of (a) device structure and (b) the corresponding energy level of the OLED

The film thickness was monitored by a quartz crystal oscillation thickness monitor. The current, voltage, electroluminescence (EL) spectrum and brightness of the devices were measured by a computer-controlled Keithley 2400 digital source meter, a PR650 spectral scanning colorimeter and a ST-86LA brightness meter, respectively. The excitation and photoluminescence (PL) spectra of the films were measured by a Hitachi F7100 fluorescence spectrophotometer. All devices were unpackaged and measured in a closed, dark, room temperature environment.

3. Results and Discussion

3.1 Hybrid device of BCzVB blue fluorescence and $Ir(ppy)_3$ green phosphorescence

$Ir(ppy)_3$ was doped in CBP, and 0.3-nm-thick BCzVB was placed on the anode side of CBP:$Ir(ppy)_3$ layer. The appropriate doping concentration of $Ir(ppy)_3$ was obtained by checking the effect of $Ir(ppy)_3$ doping concentration on the device efficiency and chromaticity. The Fig. 3 is the EL spectrum (@20 mA/cm^2) of $Ir(ppy)_3$ doped with doping concentrations of 6%, 3%, 1%, 0.7% and 0.4%, respectively. (corresponding to devices A1, A2, A3, A4 and A5 in the experimental part). From Fig. 3, the EL spectra of the devices contain only one emission peak at ca. 508 nm from the triplet exciton transition of $Ir(ppy)_3$ molecule when the doping concentration of $Ir(ppy)_3$ is high (6%, 3% and 1%), and EL peaks at 444 and 468 nm of singlet exciton transition of BCzVB molecule

appeared, besides the EL peak at 508 nm from $Ir(ppy)_3$, with decreasing of the doping concentration of $Ir(ppy)_3$ (0. 7% and 0. 4%). Generally, there are two main mechanisms for the formation of dopant excitons in doped OLED: energy transfer and carrier capture mechanisms. Because the lowest unoccupied molecular orbital (LUMO) energy level of the dopant $Ir(ppy)_3$ (~ 2.8 eV) is lower than that of the host CBP (~ 2.0 eV), $Ir(ppy)_3$ can capture electrons and directly recombine with holes from the anode side to form excitons in CBP:$Ir(ppy)_3$ doped system. When the doping concentration is high (≥ 1%), the carriers entering the CBP:$Ir(ppy)_3$ layer are likely to be directly captured by $Ir(ppy)_3$ to produce its emission, and only a small amount of carriers can recombine in CBP to form CBP excitons. The CBP singlet exciton and triplet exciton transfer their energy to the $Ir(ppy)_3$ through Förster and Dexter energy transfer, respectively. The EL spectrum of the device only contains the phosphorescent emission of $Ir(ppy)_3$. As the doping concentration of $Ir(ppy)_3$ decreases, the carrier capture decreases, and the proportion of carriers recombining in CBP to form CBP excitons increases. In this case, the CBP singlet exciton transfers its energy to the BCzVB and $Ir(ppy)_3$ through Förster energy transfer, and the CBP triplet exciton transfers its energy to the $Ir(ppy)_3$ through Dexter energy transfer, and a small number of carriers recombine in the BCzVB to form the BczVB exciton. The energy transfer principle of BCzVB/CBP:$Ir(ppy)_3$ structure is shown in Fig. 4.

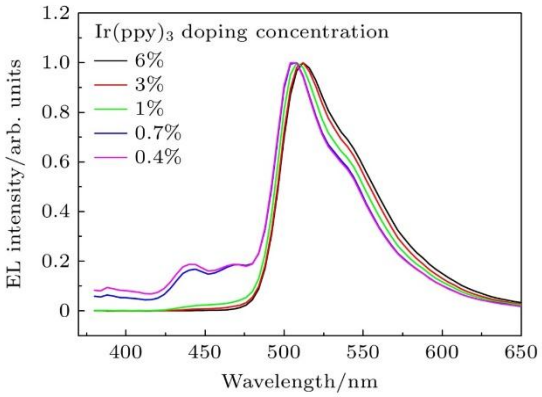

Figure 3. EL spectra (@20 mA/cm^2) of devices with different $Ir(ppy)_3$ doping concentrations (6%, 3%, 1%, 0.7%, 0.4%)

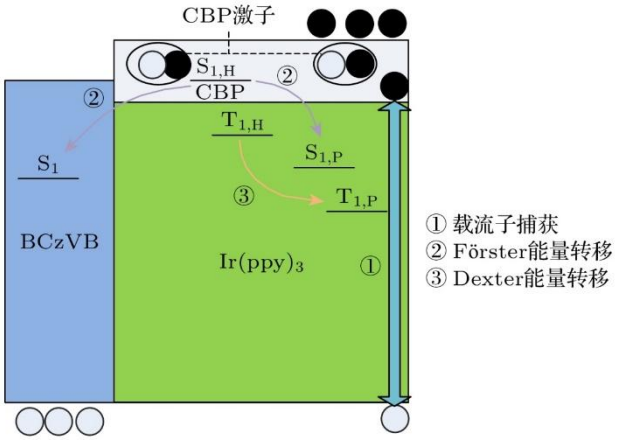

Figure 4. Schematic diagram of the energy transfer with the structure of BCzVB/ CBP:$Ir(ppy)_3$

Therefore, the exciton formation is mainly based on the mechanism of $Ir(ppy)_3$ trapping carriers, and no BCzVB emission exist as the doping concentration of $Ir(ppy)_3$ is high; the excitons form mainly in CBP, and the energy transfer process from CBP to BCzVB or $Ir(ppy)_3$ becomes dominant, resulting in the emission of BCzVB in addition to the emission of $Ir(ppy)_3$, as the doping concentration of $Ir(ppy)_3$ decreases. Naturally, the emission intensity from BCzVB increases as $Ir(ppy)_3$ doping concentration decreases, because more CBP excitons transfer energy to BCzVB.

The current efficiency-current density-brightness characteristics of the devices with different $Ir(ppy)_3$ doping concentrations (6%, 3%, 1%, 0.7% and 0.4%) are shown in Fig. 5. It can be seen from the figure that the current efficiency of the five devices decreases with the increase of current density. This is due to the fact that the higher exciton concentration at higher current density range produces TTA, and the higher driving voltage at higher current density causes the field-induced quenching[28] of excitons, and finally leads to the decrease of luminous efficiency. However, the current efficiency of devices with different doping concentrations of $Ir(ppy)_3$ decreases at different rates with the increase of current density. When the doping concentration of $Ir(ppy)_3$ is higher, the initial current efficiency is higher, but it decreases rapidly with the increase of current density; When the doping concentration of $Ir(ppy)_3$ is low, the current efficiency also decreases but the decreasing rate becomes slightly low with the increase of current density, at high current and high voltage. This actually reflects the presence of TTA between excitons, which is more likely to occur at high doping concentrations of $Ir(ppy)_3$ and less likely to occur at low doping concentrations. In addition, when the doping concentration of $Ir(ppy)_3$ is low, it is also beneficial to the energy transfer of excitons from CBP to BCzVB, which increases the blue component in the device, and is expected to be used in obtaining white light emission.

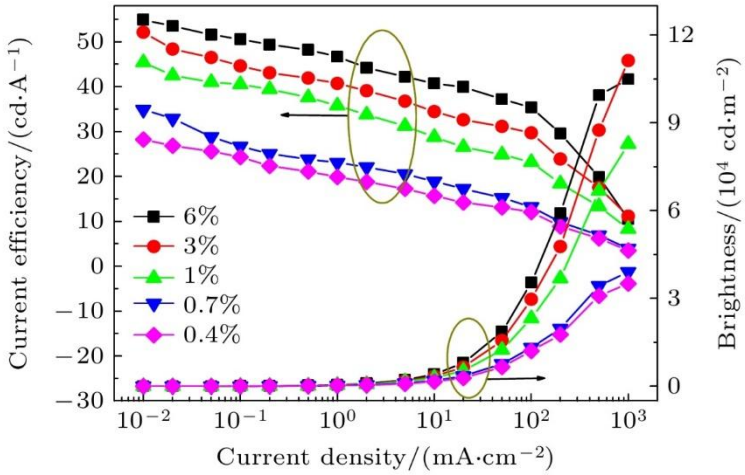

Figure 5. Current efficiency-current density-brightness characteristics of devices with different $Ir(ppy)_3$ doping concentrations (6%, 3%, 1%, 0.7%, 0.4%)

According to the above, taking into account the device efficiency and the blue light component required to generate white light, the doping concentration of $Ir(ppy)_3$ is selected to be 0.7%. In order to increase the blue light component, a device (referred to as A0) was prepared by simultaneously depositing a 0.3-nm-thick BCzVB layer on both sides of CBP:$Ir(ppy)_3$. The

structure of the device is: ITO/MoO_3 (0.05 nm)/ TAPC (50 nm)/BCzVB (0.3 nm)/CBP:$Ir(ppy)_3$ (0.7%, 20 nm)/BCzVB (0.3 nm)/TPBi (20 nm)/LiF (1.5 nm)/Al. Figure 6 shows the EL spectra of devices A0 and A4 (@ 20 mA/cm^2). It is evident that EL spectra of both devices contain emission peaks of BCzVB and $Ir(ppy)_3$, and the blue emission peak intensity of device A0 is much higher than that of device A4. The reason for this result can be explained by the energy level structure of the device. As shown in Fig. 2, the LUMO energy difference at CBP:$Ir(ppy)_3$/BCzVB interface is relatively large (~0.5 eV), and it is relatively difficult to inject electrons from BCzVB to CBP (as mentioned earlier, when $Ir(ppy)_3$ doping concentration in CBP:$Ir(ppy)_3$ is low, electrons are difficult to tunnel into the LUMO level of $Ir(ppy)_3$, and the electron migration process can be considered as injecting from the LUMO level of BCzVB into that of CBP), resulting in some electrons being intercepted by BCzVB and directly recombined with holes from the anode side to form BCzVB excitons, and additional excitons generated by energy transfer from CBP to BCzVB, these excitons undergo radiative transitions and emit light, ultimately leading to a significant increase in the blue light component of device A0. The subsequent acquisition of white light is based on the structural parameters of device A0.

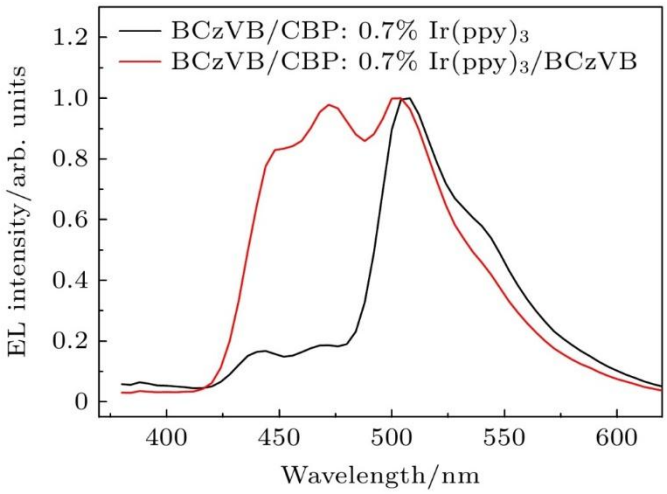

Figure 6. Comparison of EL spectra (@ 20 mA/cm^2) of devices with BCzVB deposited on both and one sides at a $Ir(ppy)_3$ doping concentration of 0.7%

To illustrate the energy transfer between CBP and BCzVB or $Ir(ppy)_3$, thin films of CBP (20 nm), CBP:$Ir(ppy)_3$ (0.7%, 20 nm), and BCzVB (0.3 nm)/CBP:$Ir(ppy)_3$ (0.7%, 20 nm)/BCzVB (0.3 nm) were prepared on glass substrates. The thickness of each film was almost the same, namely 20 nm, corresponding to the structure and thickness of the active layer in the device. The excitation and PL spectra were respectively shown in Fig. 7. The absorption spectra of the three films are similar, but the PL spectra are quite different: the only existed emission from CBP in CBP film, emissions from both CBP and $Ir(ppy)_3$ in CBP:$Ir(ppy)_3$ film, emissions from both CBP, $Ir(ppy)_3$ and BCzVB in the BCzVB/CBP:$Ir(ppy)_3$/BCzVB film. The amount (mass or molar) of CBP in the three films is more than 90%. According to the rule that the absorbance of the material is proportional to its amount, it can be judged that the excitation spectrum is mainly contributed by CBP, which is consistent with the above experimental results. For the PL, if there is no energy transfer between CBP and BCzVB and $Ir(ppy)_3$, the PL spectra of the three films should also be dominated by the

emission of CBP, because the contribution of $Ir(ppy)_3$ and BCzVB to the luminescence should be less than 5%, which can be ignored. However, the experimental results show that there is a significant phosphorescence of $Ir(ppy)_3$ in the above CBP:$Ir(ppy)_3$ film, and there is a considerable phosphorescence of $Ir(ppy)_3$ and fluorescence of BCzVB in the BCzVB/CBP:$Ir(ppy)_3$/BCzVB film. It shows that the effective energy transfer can occur between CBP and BCzVB or $Ir(ppy)_3$. However, when the amount of $Ir(ppy)_3$ and BCzVB is small, the emissions from $Ir(ppy)_3$ and BCzVB produced by energy transfer is also limited, so there is still more residual emission of CBP in the latter two films. However, the energy transfer efficiency of the same film system in EL devices is different due to the difference between the exciton formation regions in EL and PL processes. In EL devices, the exciton is formed near the interfaces, and the energy acceptor BCzVB is just near the interfaces, so the energy transfer efficiency is naturally very high. This is confirmed by the weak emission from CBP seen in the EL devices.

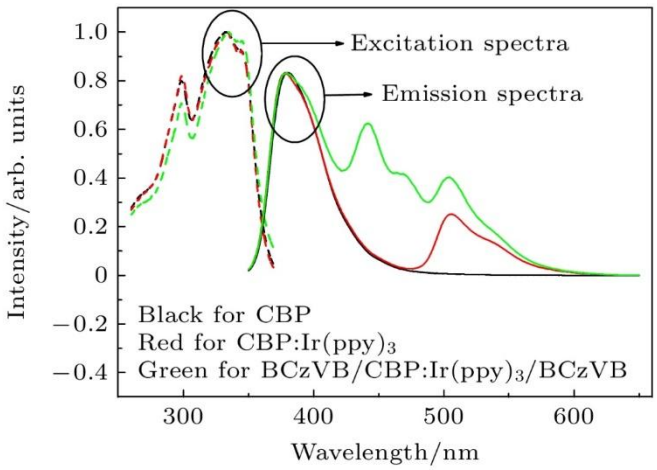

Figure 7. Excitation and PL spectra of CBP (20 nm), CBP:$Ir(ppy)_3$ (0.7%, 20 nm) and BCzVB (0.3 nm)/CBP:$Ir(ppy)_3$ (0.7%, 20 nm)/BCzVB (0.3 nm) film

3.2 Optimize the insertion position of DCM

A 0.3-nm-thick DCM layer was inserted into CBP:$Ir(ppy)_3$ layer at different positions, and the influence of the insertion position of DCM on the proportion of each color was investigated, and the appropriate insertion position was determined to achieve white light emission. Different devices were prepared for comparison by selecting the distance between the DCM insertion position and the anode side interface of CBP:$Ir(ppy)_3$, i.e., TAPC/BCzVB/CBP:$Ir(ppy)_3$ interface, to be y = 10,12,14,16 nm, respectively (corresponding to devices B1, B2, B3 and B4 in the experimental part). The EL spectra of different devices at a current density of 20 mA/cm^2 are shown in Fig. 8 (normalized according to the emission peak of $Ir(ppy)_3$). It can be seen from the figure that there are three emission peaks in the spectra, which are located near 448, 508 and 572 nm, corresponding to blue, green and red colors, respectively. The emission peak near 448 nm is due to the transition of singlet exciton of BCzVB molecule, that near 508 nm is due to the transition of triplet exciton of $Ir(ppy)_3$ molecule, and that near 572 nm is from the transition of singlet exciton of DCM molecule. As the insertion site of DCM in CBP:$Ir(ppy)_3$ moves toward the cathode, the

intensity of the emission peak from BCzVB decreases and that from DCM increases. As mentioned above, the LUMO energy level difference at the CBP:Ir(ppy)$_3$/BCzVB interface is large, so that part of the electrons entering BCzVB layer are trapped and directly recombine with the holes to form BCzVB excitons. Part of the BCzVB excitons emit light through radiative transition, and the other part transfers energy to the DCM through Förster energy transfer. Some of the electrons entering the CBP:Ir(ppy)$_3$ layer are captured by Ir(ppy)$_3$ and recombine with the holes to form Ir(ppy)$_3$ excitons, while the other part recombine with the holes in the CBP to form CBP excitons. Ir(ppy)$_3$ excitons can emit light through radiative transition or transfer its energy to the DCM through Förster type energy transfer (phosphorescence sensitization), the CBP singlet exciton transfers its energy to BCzVB and DCM through this type energy transfer, and the CBP triplet exciton transfers its energy to Ir(ppy)$_3$ through Dexter type energy transfer. For device B1 (DCM ultrathin layer is located at y = 10 nm), DCM is far away from BCzVB layer at the cathode side and the energy transfer ratio from BCzVB to DCM is relatively low, at which point the emission from BCzVB is the strongest and that from DCM is the weakest. When the insertion position of DCM moves to the cathode side, the distance between DCM and BCzVB decreases, and the proportion of energy transfer from BCzVB exciton to DCM increases gradually. At this time, the emission intensity of BCzVB decreases and the emission intensity of DCM increases gradually. The energy transfer principle of BCzVB/CBP:Ir(ppy)$_3$/DCM/CBP:Ir(ppy)$_3$/BCzVB structure is shown in Fig. 9. Note that the EL spectra in Fig. 8 have been normalized based on the emission peak of Ir(ppy)$_3$, the above analysis of the intensity change of DCM emission peak is carried out relative to that of Ir(ppy)$_3$, which cannot reflect the actual change of DCM emission peak.

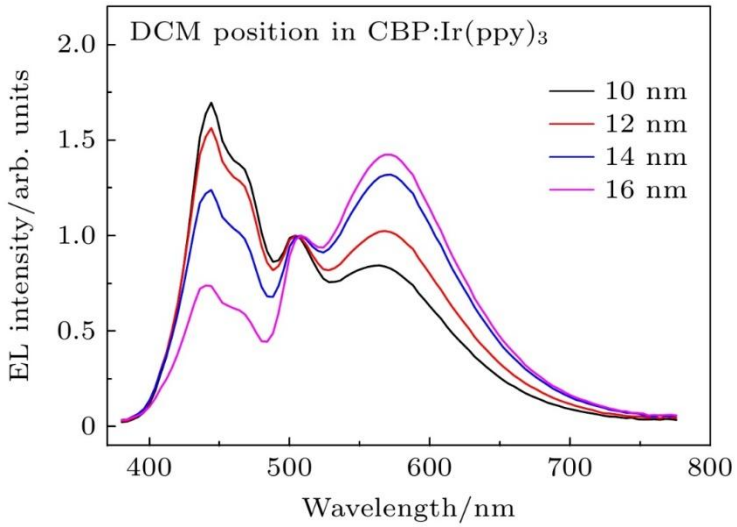

Figure 8. EL spectra (@20 mA/cm^2) of devices with ultra-thin DCM layer in CBP:Ir(ppy)$_3$ at distances of y = 10, 12, 14, 16 nm, respectively, from the (+) BCzVB/CBP:Ir(ppy)$_3$ interface at anode side

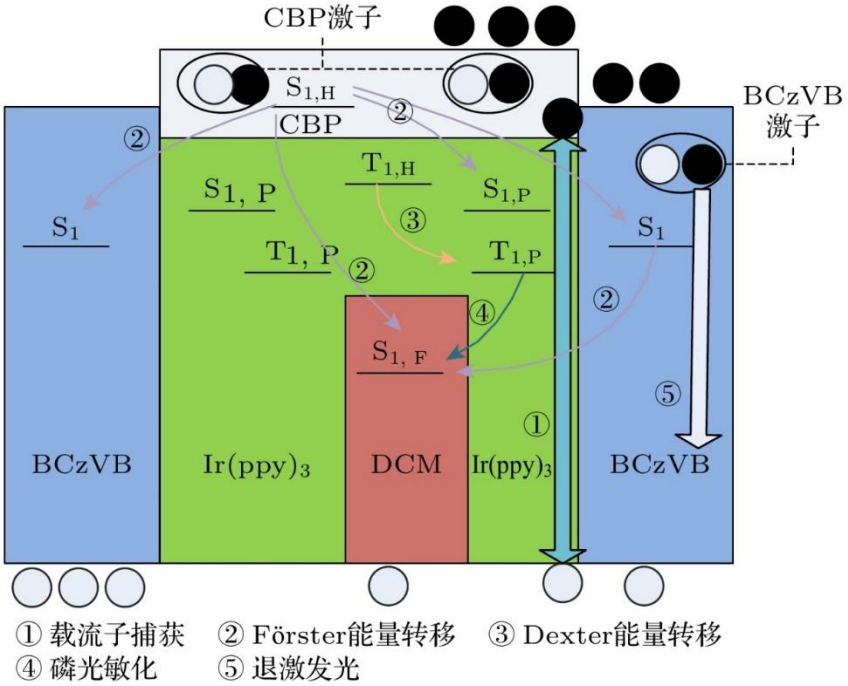

Figure 9. Schematic diagram of the energy transfer with the structure of BCzVB/CBP:Ir(ppy)$_3$/ DCM/CBP:Ir(ppy)$_3$/BCzVB

The Fig. 10 is the comparison of the performances of devices with DCM in CBP:Ir(ppy)$_3$ layer at different positions (y = 10, 12, 14, 16 nm). It can be seen from the Fig. 10(a) that the difference of the current density-voltage characteristic curves of each device is small, which indicates that changing the DCM position has little effect on the transport of carriers in the device. As shown in the Fig. 10(b), the current efficiency of the device decreases with increasing current density. This is similar to that in Fig. 5, which is the efficiency drop caused by field quenching. At the same current density, the current efficiency of the device decreases with the movement of the insertion position of DCM toward the cathode. At a current density of 1 mA/cm^2, the current efficiencies of the devices were 3.09, 2.73, 2.4 and 2. 03 cd/A, respectively, and the corresponding brightness were 30.9, 27.3, 24 and 20.3 cd/m^2, respectively. The reason for this result can be attributed to the fact that the DCM molecule itself is prone to produce concentration quenching[29], at high exciton concentrations, so the efficiency of the device decreases gradually although DCM obtains more energy transfer from BCzVB to produce more excitation. The DCM ultra-thin layer achieved the highest EQE of 2.5% (current efficiency of 5.1 cd/A) at a current density of 0.02 mA/cm^2 and the highest brightness of 12400 cd/m^2 at a current density of 1000 mA/cm^2 in a device with y=10 nm. The CIE color coordinates at a current density of 1 mA/cm^2 of the device with DCM ultra-thin layer located at y=12 nm are (0.33, 0.33), achieving the ideal white light equilibrium point

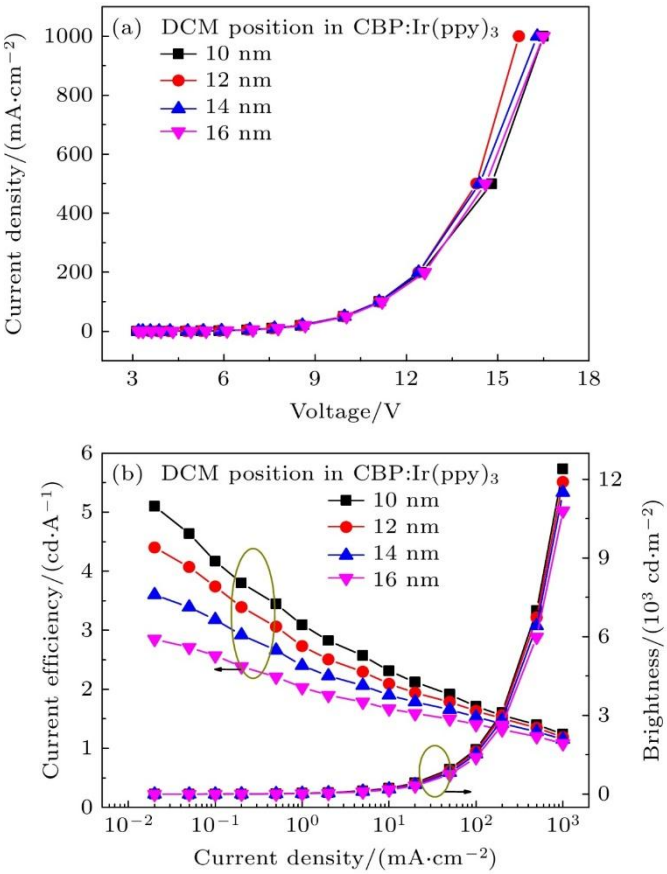

Figure 10. Current density-voltage (a) and current efficiency-current density-brightness (b) characteristics of devices with ultra-thin DCM layer in CBP:Ir(ppy)$_3$ at distances of y = 10, 12, 14, 16 nm, respectively, from the (+) BCzVB/CBP:Ir(ppy)$_3$ interface at anode side

In general, the exciton recombination region in a white light-emitting device with a multilayer structure may change with the change of voltage or current, and the emissive properties of different luminescent materials may also change, resulting in the change of the luminescent color and spectrum of the device. EL spectra of device B2 (y = 12 nm) at different current densities are plotted in Fig. 11. It can be seen that the relative intensity of blue and red spectra is close, and the multi-component emission is more balanced at small current density or voltage region. With the increase of current density or voltage, the intensity of green and red emission peaks decreases gradually relative to the blue emission, which can be attributed to the fact that Ir(ppy)$_3$ and DCM have more serious concentration-quenching effect than BCzVB, because the green emission of Ir(ppy)$_3$ originates from the transition of its long-lived triplet exciton, while the singlet excitation of DCM mostly originates from the energy transfer of Ir(ppy)$_3$ triplet exciton, whose lifetime is also longer than that of pure singlet exciton. The CIE color coordinates of the devices corresponding to y = 10,12,14,16 nm at different current densities are listed in Tab. 1. The CIEx and CIEy color coordinates of each device decrease in different degrees with the increase of current or voltage. Tab. 2 is a summary of the performance of all OLED devices. It can be seen that in the process of obtaining white light, the efficiency loss of the device is large. The reason may be attributed to the fact that the CBP host material fails to effectively transfer the singlet exciton energy to the blue luminescent material BCzVB due to the existence of Ir(ppy)$_3$, while the Ir(ppy)$_3$ green

phosphorescent material has to choose a lower doping concentration, which greatly reduces the triplet exciton harvest, coupled with the quenching property of DCM, resulting in the low efficiency of the device. It is expected that the efficiency will be further improved by screening suitable host materials, adjusting and optimizing the exciton recombination region, and selecting red fluorescent materials with better performance.

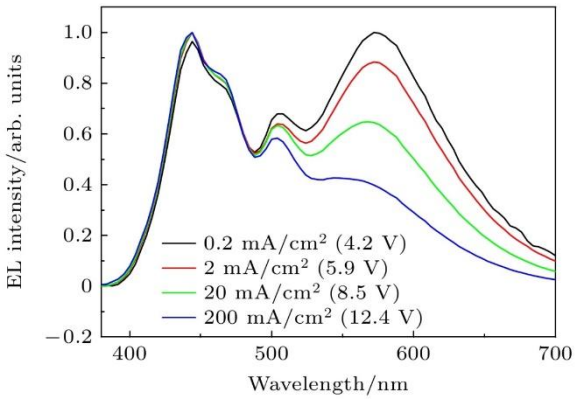

Figure 11. EL spectra of the device with *y* = 12 nm at different current density (voltage)

Table 1. Variation of CIE color coordinates of devices with *y* = 10, 12, 14, 16 nm (@0.2–200 mA/cm^2)

Device	CIE color coordinate variation range
B1 (*y* = 10)	(0.28—0.22, 0.32—0.21)
B2 (*y* = 12)	(0.34—0.23, 0.36—0.23)
B3 (*y* = 14)	(0.41—0.25, 0.40—0.26)
B4 (*y* = 16)	(0.46—0.27, 0.43—0.31)

Table 2. Summary of the EL performances of the OLED

Device	Maximum current efficiency/(cd·A^{-1})	Maximum luminance/(cd·m^{-2})
A0 (*x* = 0.7)	9.53	23760
A1 (*x* = 6)	54.9	104900
A2 (*x* = 3)	52.1	111276
A3 (*x* = 1)	45.4	82830
A4 (*x* = 0.7)	34.9	39072
A5 (*x* = 0.4)	28.2	35046
B1 (*y* = 10)	5.1	12400
B2 (*y* = 12)	4.4	11900
B3 (*y* = 14)	3.6	11500
B4 (*y* = 16)	2.85	10800

4. Conclusion

In summary, phosphor-sensitized fluorescent white organic electroluminescent devices were prepared by combining ultra-thin layers and doping scheme, white luminescence was obtained by

changing the insertion position of the DCM ultra-thin layer, with a maximum external quantum efficiency of 2.5% (current efficiency of 5.1 cd/A) and a maximum brightness of 12400 cd/m^2. The CIE color coordinates of device B2 (DCM located at y=12 nm) have reached the ideal white light equilibrium point (0.33, 0.33) at a current density of 1 mA/cm^2. Through phosphorescence sensitizing fluorescence, the triplet excitons of phosphorescent materials can transfer energy to fluorescent materials to reduce TTA. However, due to the severe concentration quenching of DCM, the improvement of device performance is limited, and more suitable red fluorescent materials need to be further searched

References

[1] Kido J, Hongawa K, Okuyama K 1994 *Appl. Phys. Lett.* **64** 815

[2] Wu Y T, Zhu H Q, Wei F X, Wang H Y, Chen J, Ning Y R, Wu F J, Chen X L, Xiong Z H 2022 *Acta Phys. Sin.* **71** 227201

[3] Hwang J, Choi H K, Moon J, Kim T Y, Shin J W, Joo C W, Han J H, Cho D H, Huh J W, Choi S Y, Lee J I, Chu H Y 2012 *Appl. Phys. Lett.* **100** 133304

[4] Cho J T, Kim D H, Koh E I, Kim T W 2014 *Thin Solid Films* **570** 63

[5] Chen Y W, Yang D Z, Qiao X F, Dai Y F, Sun Q, Ma D G 2020 *J. Mater. Chem. C* **8** 6577

[6] Rosenow T C, Furno M, Reineke S, Olthof S, Lüssem B, Leo K 2010 *J. Appl. Phys.* **108** 113113

[7] Wang Q, Ding J Q, Ma D G, Cheng Y X, Wang L X, Jing X B, Wang F S 2009 *Adv. Funct. Mater.* **19** 84

[8] Sun Y, Forrest S R 2007 *Appl. Phys. Lett.* **91** 263503

[9] Reineke S, Schwartz G, Walzer K, Falke M, Leo K 2009 *Appl. Phys. Lett.* **94** 163305

[10] Gao Z X, Wang F F, Guo K P, Wang H, Wei B, Xu B S 2014 *Opt. Laser Technol.* **56** 20

[11] Murawski C, Leo K, Gather M C 2013 *Adv. Mater.* **25** 6801

[12] Reineke S, Schwartz G, Walzer K, Leo K 2007 *Appl. Phys. Lett.* **91** 123508

[13] Baldo M A, Thompson M E, Forrest S R 2000 *Nature* **403** 750

[14] Heimel P, Mondal A, May F, Kowalsky W, Lennartz C, Andrienko D, Lovrincic R 2018 *Nat. Commun.* **9** 4990

[15] D'Andrade B W, Baldo M A, Adachi C, Brooks J, Thompson M E, Forrest S R 2001 *Appl. Phys. Lett.* **79** 1045

[16] Chen X, Huang Y, Luo D, Chang C, Lu C, Su H 2023 *Chem. Eur. J.* **29** e202300034

[17] Baek S, Park J Y, Woo S, Lee W, Kim W, Cheon H, Kim Y, Lee J 2024 *Small Struct.* **5** 2300564

[18] Cheong K, Han S W, Lee J Y 2024 *Small Methods* **8** 2301710

[19] Liang N, Zhao Y K, Wu Y Z, Zhang C R, Shao M 2021 *Appl. Phys. Lett.* **119** 053301

[20] Zhou Y, Gao H, Wang J, Yeung F S Y, Lin S H, Li X B, Liao S L, Luo D X, Kwok H S, Liu B Q 2023 *Electronics* **12** 3164

[21] Meyer J, Hamwi S, Kröger M, Kowalsky W, Riedl T, Kahn A 2012 *Adv. Mater.* **24** 5408
[22] Vipin C K, Shukla A, Rajeev K, Hasan M, Lo S C, Namdas E B, Ajayaghosh A, Unni K N N 2021 *J. Phys. Chem. C* **125** 22809
[23] Yang S H, Huang S F, Chang C H, Chung C H 2011 *J. Lumin.* **131** 2106
[24] Ko C W, Tao Y T, Lin J T, Justin Thomas K R 2002 *Chem. Mater.* **14** 357
[25] Petrova P K, Ivanov P I, Tomova R L 2014 *J. Phys.: Conf. Ser.* **558** 012028
[26] Miao Y Q, Du X G, Wang H, Liu H H, Jia H S, Xu B S, Hao Y Y, Liu X G, Li W L, Huang W 2014 *RSC Adv.* **5** 4261
[27] Zou W J, Wu Y Z, Zhang C R 2024 *J. Lanzhou Univ. Tech.* **50** 21
[28] Gulbinas V, Zaushitsyn Y, Sundström V, Hertel D, Bässler H, Yartsev A 2002 *Phys. Rev. Lett.* **89** 107401
[29] Liu Z G, Chen Z J, Gong H Q 2005 *Chinese Phys. Lett.* **22** 1536